Low Temperature Physics/Fizika Nizkikh Temperatur, 2014, v. 40, No. 7, pp. 801–806

Magnetic field penetration in MgB_2 single crystals: pinning and Meissner holes

V. Chabanenko[1], E. Kuchuk[1], V.V. Yurchenko[2], P. Mikheenko[2], I. Abal'osheva[3], R. Cortés-Maldonado[4], F. Pérez-Rodríguez[4], J. Karpinski[5,6], N.D. Zhigadlo[5], S. Katrych[6], and R. Puźniak[3]

[1] *A. Galkin Donetsk Institute for Physics and Engineering, NASU, Donetsk 83114, Ukraine*
E-mail: vikchabanenko@gmail.com

[2] *Department of Physics, University of Oslo, P.O. Box 1048, Blindern 0316, Oslo, Norway*

[3] *Institute of Physics, Polish Academy of Sciences, Aleja Lotników 32/46, Warsaw 02-668, Poland*

[4] *Instituto de Física, Benemérita Universidad Autónoma de Puebla, Puebla, México*

[5] *Laboratory for Solid State Physics, ETH Zurich, Zurich 8093, Switzerland*

[6] *Institute of Condensed Matter Physics, EPFL, Lausanne 1015, Switzerland*

Received February 17, 2014, published online May 21, 2014

The evolution of flux distribution in MgB_2 single crystals during their remagnetization was imaged with magneto-optical technique. Meissner holes, formed as the areas where the annihilation of vortices and antivortices takes place, were found at the boundary between oppositely magnetized parts of the crystal. Gradient of magnetic induction in the vicinity of Meissner holes was found to be enhanced. Finger-like structures of convex shape, formed during the penetration of magnetic flux inside the crystal, were observed and explained as an effect of inhomogeneous pinning and demagnetizing field redistribution in the sample.

PACS: 74.25.Ha Magnetic properties including vortex structures and related phenomena;
78.20.Ls Magnetо-optical effects;
74.25.Wx Vortex pinning (includes mechanisms and flux creep).

Keywords: magnetooptic of flux penetration, vortices, antivortices, Meissner holes, inhomogeneous pinning, single crystal MgB_2.

1. Introduction

The magneto-optical imaging (MOI) allows tracking magnetic flux distribution close to the sample surface [1,2]. The numerical inversion of Biot–Savart law gives an integral relation between the current density distributions and the magnetic self-field. It opened up the possibility of finding supercurrent distributions by MOI. The MOI technique permits the investigation of complex problems, such as inhomogeneous and anisotropic current flow, the dependence of critical current on the local magnetic field, the current distribution around crystal defects such as grain boundaries and inner interfaces [1] etc. The MOI studies of the vortex dynamics in Nb films [3] and foils [4] reveal stochastic jumps of the flux bundles forming a rough penetration front and giant abrupt changes in the magnetic-flux distribution as a result of the collapse of critical state. For MgB_2, most of the studies were devoted to the avalanches in thin films [5,6] and limited data only are available on magnetic field penetration into MgB_2 crystals [7,8]. This is mainly due to the difficulties in growing large in size perfect crystals.

Here the magnetic induction patterns at the boundary between oppositely magnetized parts of MgB_2 crystals are studied in details. It was found that near the edge of the crystal the field of opposite directions is present and Meissner holes — the areas where the annihilation of neighboring vortices and antivortices occurs and the regions free from flux cavity appear [9,10] — are formed (Fig. 1).

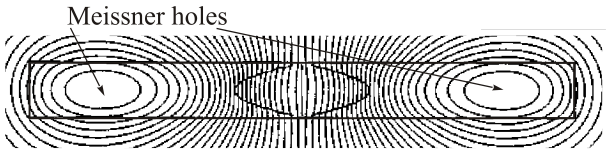

Fig. 1. Magnetic field lines during the penetration of flux of opposite orientation, occurring when the external field H is decreased again after it had first been increased to the field of full penetration H_p. Meissner holes show on a normally remagnetized plate (after E.H. Brandt [10]).

2. Experiment and samples

The magnetic flux distribution was imaged and analyzed using MOI technique during remagnetization of MgB_2 crystals. This technique provides data for the normal component of magnetic induction B_n close to the sample surface. As the MOI technique is also a sensitive tool for investigations of crystal inhomogeneity associated with the imperfections of structure and composition [2,11], it allowed us to study longitudinal and transverse cross sections of the finger-like structures formed during magnetic flux penetration in weak spots close to the edge of the crystal.

The measurements were performed at the temperature range of ~ 3–40 K during the magnetization process in magnetic field up to 100 mT and during reversal magnetization with the change of direction of the field.

The studied crystals were grown from a MgB_2 solution at the pressure of 15 kbar and the temperature of 1800 °C in a special high-pressure chamber, which allowed the growth of samples at pressure up to 35 kbar and temperatures up to 2200 °C [12]. Here we show data obtained on the crystal S1 of the approximate dimensions 860×660×250 μm that has the *c*-axis normal to the platelets and on disc-shaped crystal S2 with 500 μm in diameter and thickness of ~150 μm. The external magnetic field was applied in direction perpendicular to the sample surface.

Figure 2 shows electron microscope images of MgB_2 plate-like sample S1 with fine details of the shape and the structure of the crystal, presented with enhanced magnifications in Figs. 2(b)–(d). According to the above images sample S1 has a complex shape with nonplanar sides. The steps seen in the crystal may be a source of significant pinning of magnetic flux.

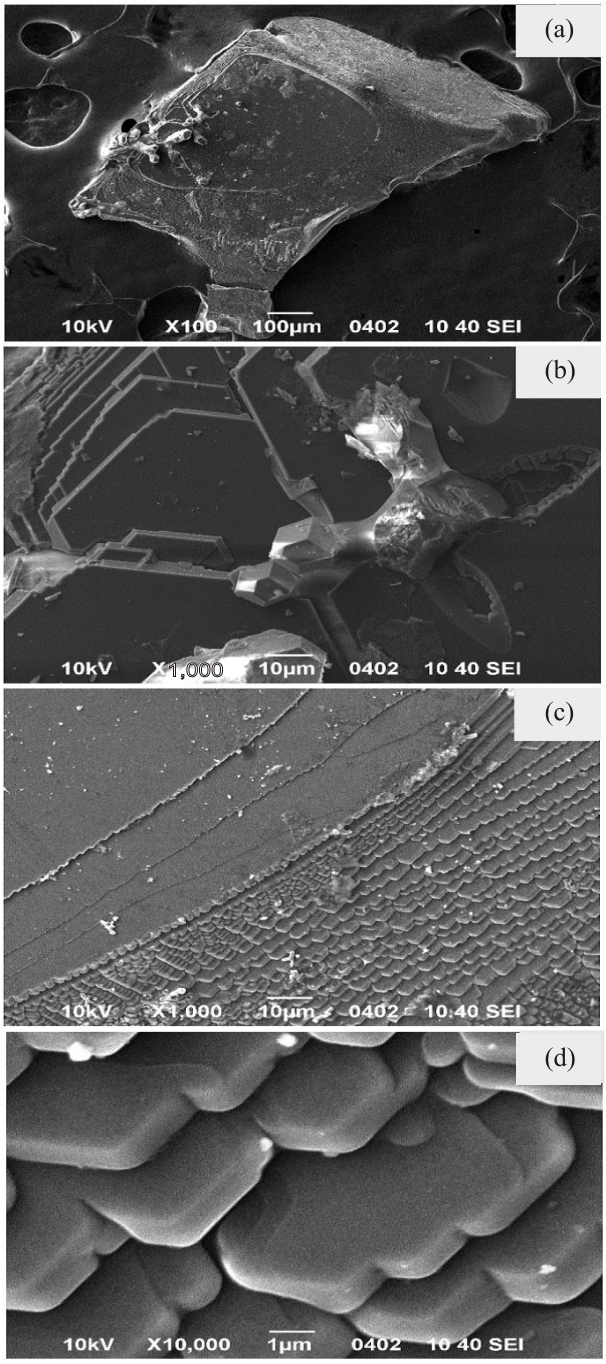

Fig. 2. Electron microscope images of MgB_2 plate-like crystal S1. The steps between the plates of the crystal are clearly seen.

3. Results and discussion

3.1. Magnetization process

Figure 3 shows penetration of magnetic field into the crystal S1. Magneto-optical imaging is an effective tool in revealing field distribution in the surrounding of defects, while not all defects (inhomogeneities) can be detected by the optical or electron microscope imaging. Summarizing obtained results: At the 20 K (Fig. 3(c)), we can find the regions of the crystal (see, red square), where the penetration of the field inside of the sample is more or less uniform, almost homogeneous until the middle of the sample. Here, the crystal is quite perfect, pinning centers are weak, and the critical current is low. Areas on the right and the left side of the crystal are characterized by highly inhomogeneous penetration, and in some places (black areas), almost complete shielding appear. Here, crystal defects act as strong pinning centers and therefore, significant critical

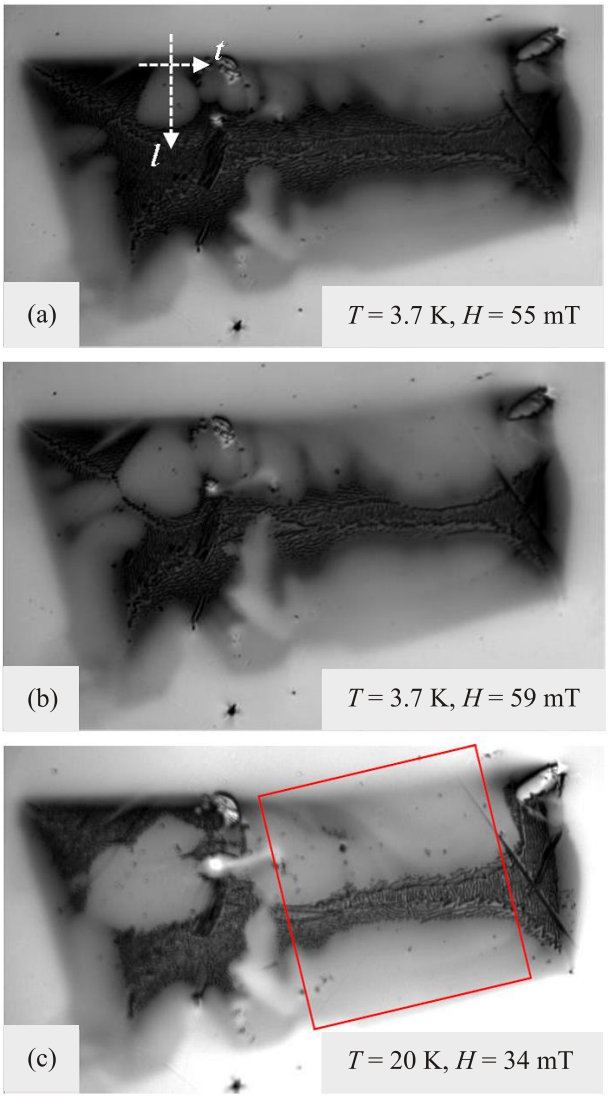

Fig. 3. (Color online) The magnetic flux penetration into the crystal S1. The flux profile in the area of finger-like penetration is analyzed in direction perpendicular to the sample surface (*l*-direction) and along top edge of the sample (*t*-direction).

currents exceeding 5–10 times of the value in the red square area may appear.

In the left part of the crystal, close to its top edge, there are spots with weak reduced superconducting parameters, where magnetic flux enters the sample easier than in other places. After entering, magnetic flux propagates in a diffuse manner forming finger-like patterns that are clearly seen near the top edge of the sample in Fig. 3. These patterns remind those seen in superconducting films with quite strong pinning and in $YBa_2Cu_3O_x$ crystals [11]. It reveals significant pinning in the crystal. The origin of pinning could be in the attraction of vortices due to the steps seen in Fig. 2.

One can also see that top left part of the sample remains in Meissner state. The penetration of the field in right part is quite homogeneous and this area was used for investigation of the process of magnetization and demagnetization of the sample applying positive and then negative magnetic field.

In a specific range of the field, transverse (*t*-direction, Fig. 3(a)) and longitudinal (*l*-direction) profiles of the magnetic induction were analysed in a finger-like structures shown in Fig. 3. The profiles recorded in the increasing positive field are shown in Fig. 4. One can see that the distribution of magnetic flux has a convex dome-like shape both in longitudinal and transverse directions. Increase of the field leads to increase of both height and width of the domes. The gate, or the weak spot, where flux enters the crystal becomes wider with the increase of the field.

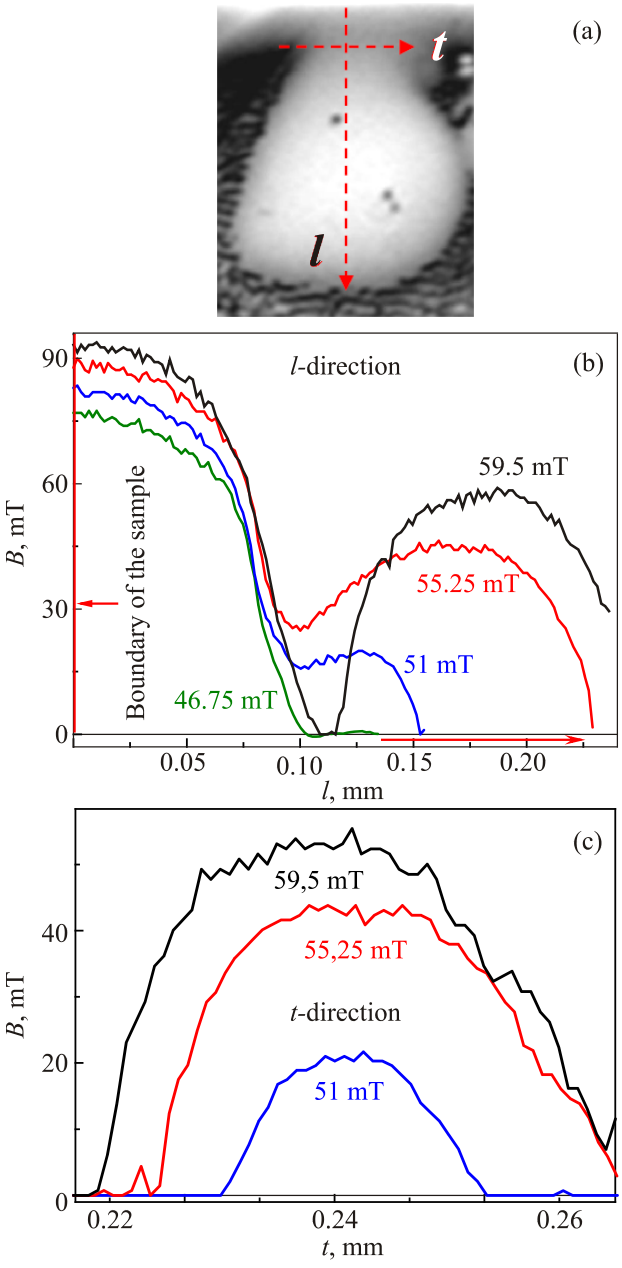

Fig. 4. (Color online) Profiles of magnetic induction *B* in *l*- (b) and *t*-directions (c) of the finger-like structure shown in the upper panel (a).

The formation and growth of dome-like areas containing magnetic flux reflects presence of edge defects and reasonably strong pinning inside the crystal, which restricts further motion of magnetic fluxes. The similar induction profiles observed in $YBa_2Cu_3O_x$ crystals [11] were interpreted as flow of flux into central zone, characterized by weak pinning. When magnetic field further increases, the flux moves into the central part erasing the flux free area.

3.2. Flux trapping and remagnetization in negative field

Figure 5 shows typical magneto-optical images recorded at temperature of 3.66 K. Flux trapped as a result of magnetization of the sample in 85 mT and switching off the field to $H = 0$ is shown in Fig. 5(a). The images 5(b) and (c) show distribution of flux after application of negative fields of $H = -17$ mT and -28.9 mT, respectively. Brighter intensity in these images corresponds to a higher normal component of magnetic induction (B_n) and the darker one to lower B_n. The white arrow in Fig. 5(a) shows the direction along which the magnetic flux distribution was analyzed.

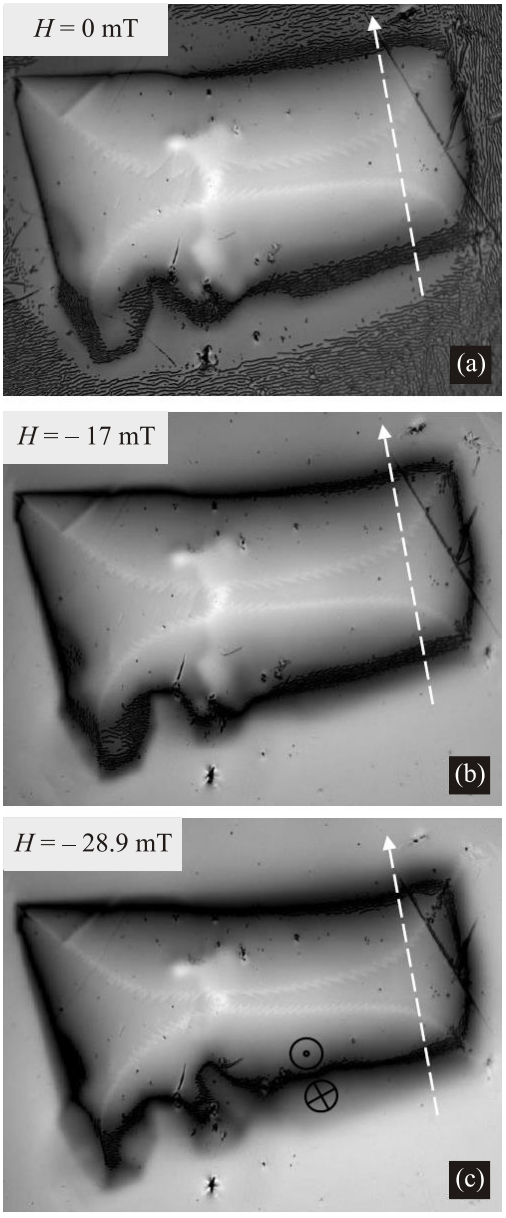

Fig. 5. Magneto-optical images of MgB_2 crystal S1 at $T = 3.66$ K during remagnetization in negative fields H, mT: 0 (a); –17 (b); –28.9 (c). The boundary between up (⊙) and down (⊕) magnetized areas is near of the crystal edges (c).

The remagnetization front reveals Meissner hole as a dark line around the perimeter of the sample, as it is shown in the panels of Fig. 5. With increase of negative field, Meissner hole moves inside the crystal and its width decreases (Fig. 6). The Meissner hole in zero magnetic field (Fig. 5(a)) occurs due to finite demagnetization factor of the crystal and to the ability of the crystal to trap magnetic field. Figure 7 shows the profiles of the normal magnetic induction B_n for different applied fields along the direction marked by the white line in Fig. 5(a). It appears that in the vicinity of the parts of Meissner hole (squares in the figure) the derivative dB_n/dx is increased by 2–3 times compared to its value in the bulk, controlled by the pinning.

This is in agreement with model developed in Ref. 9 (Fig. 4(a)) and Ref. 10, showing that the Meissner hole

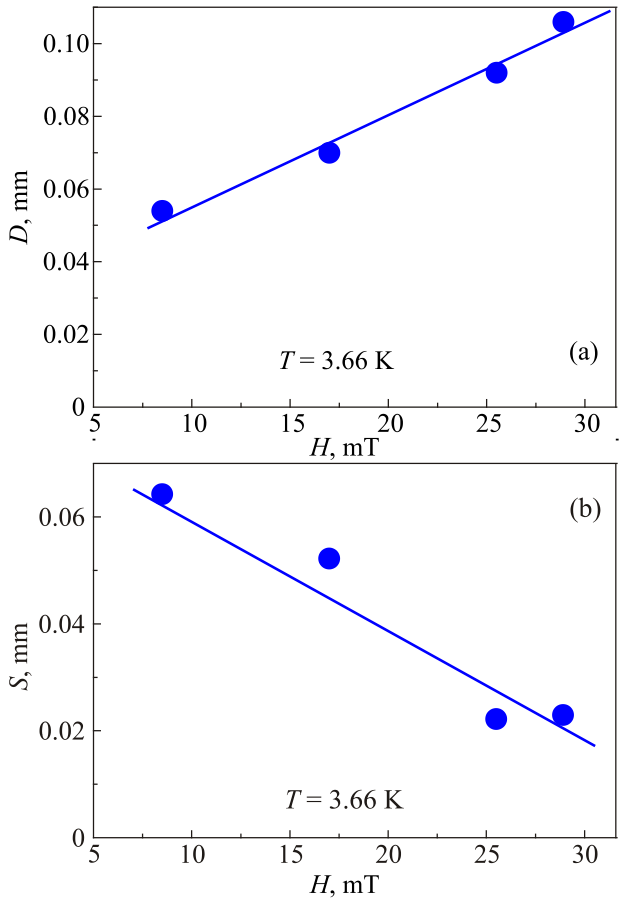

Fig. 6. Effect of increasing negative magnetic field on Meissner hole displacement inside the crystal (a) and on its width (b).

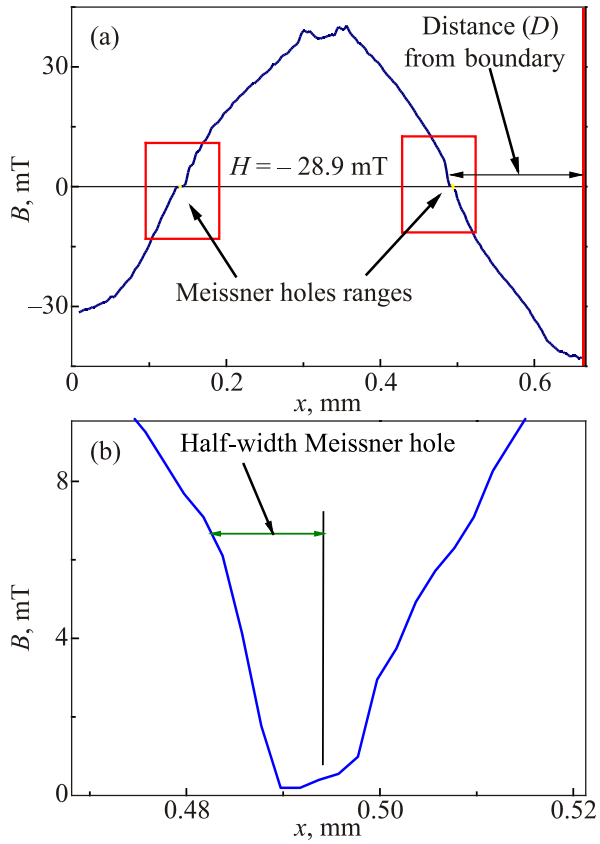

Fig. 7. (a) Profile of trapped magnetic flux after magnetization in $H = 85$ mT at $T = 3.66$ K; (b) Absolute value of magnetic induction in the vicinity of right "projection" of Meissner hole in panel (a).

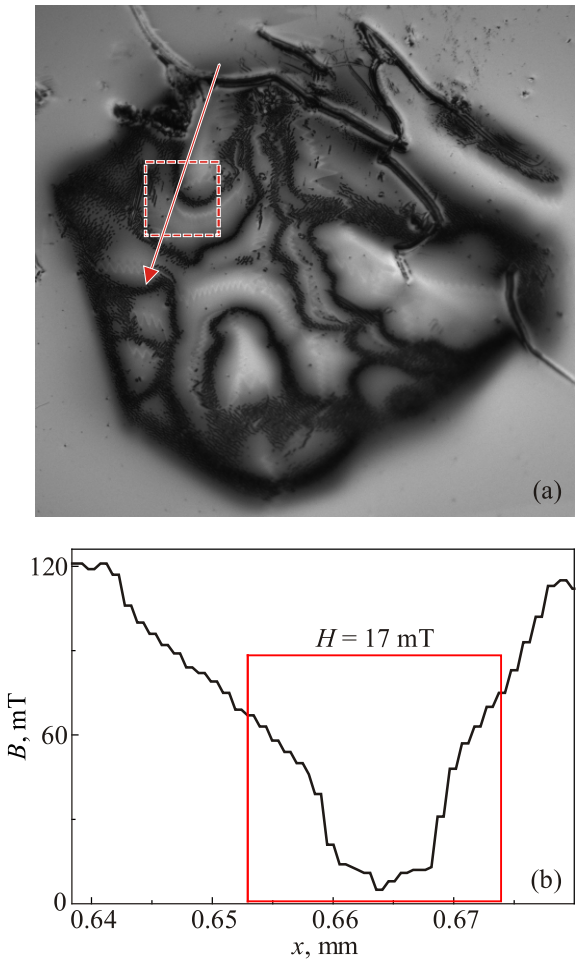

Fig. 8. (a) Nut-like pattern in crystal S2 constituted by Meissner holes in field of 17 mT; (b) Magnetic induction profile (absolute value) along the line shown by large arrow in (a). The structure of induction around the Meissner hole is marked by square.

displaces magnetic flux to the periphery [9 (Fig. 3(a))] of the area where annihilation of vortices and anti-vortices takes place. The displaced flux increases B_n in the area close to the hole.

3.3. Nut-like structure distribution of magnetic flux in the crystal

Figure 8(a) shows nut-like structure formed by Meissner holes in crystal S2. Presented image was obtained by exposing sample to magnetic field of a value above full penetration field. After that the direction of the field was reversed setting its absolute value somewhat below the value of previous field. This procedure was repeated several times, finally reducing field to 17 mT.

The structure in Fig. 8(a) is similar to that obtained in $YBa_2Cu_3O_x$ crystal in the presence of the ac field [10]. The Meissner holes in such a structure separate domains with opposite directions of magnetic field. An example of the profile of the absolute value of induction in the vicinity of one of the holes is shown in Fig. 8(b). Image is taken along the line marked by large red arrow in Fig. 8(a). As in Fig. 7(b), there is increase in the gradient of induction in the vicinity of the hole.

The nut-like structure in Fig. 8(a) shows several areas with strong pinning separated by areas of weaker pinning. Such a structure deserves further investigation of its local magnetic properties in combination with structural analysis.

4. Conclusions

As a result of the application of MOI technique to MgB_2 single crystals it was found that:

— Meissner holes are formed along the edge of the crystal in the trapped magnetic field or in the field of the opposite polarity to the field used for magnetization;

— in agreement with available models, Meissner holes are shifted towards the centre of the crystal;

— the derivative of magnetic induction dB_n/dx in the vicinity of Meissner hole is 2–3 times larger than the bulk value, controlled by pinning;

— structure formed by Meissner holes in a bulk crystal is similar to "fingerprints", unlike that one of thin films, where dendritic structures are dominant;

— the induction profiles of finger-like structures in longitudinal and transverse directions have a convex dome-like shape;

— the gates, through which magnetic flux enters the crystals widen with an increase of external magnetic field.

Acknowledgments

This work was partially supported by SEP-CONACYT (Mexico) under grant CB-2012-01-183673, by the National Science Centre of Poland based on decision No. DEC-2013/08/M/ST3/00927, and by Swiss National Science Foundation. J.K and S.K acknowledge support of European Community FP7 Project Super-Iron. Authors wish to thank V.V. Burkhovetskii for electron microscope images of crystals.

1. A. Polyanskii, D.M. Feldmann, and D.C. Larbalestier, in: *Handbook of Superconducting Materials*, D. Cardwell and D. Ginley (eds.), Institute of Physics Publishing, Bristol (1999).
2. Ch. Jooss, J. Albrecht, H. Kuhn, S. Leonhardt, and H. Kronmüller, *Rep. Prog. Phys.* **65**, 651 (2002).
3. V.K. Vlasko-Vlasov, U. Welp, V. Metlushko, and G.W. Crabtree, *Phys. Rev. B* **69**, 140504(R) (2004).
4. R. Prozorov, D.V. Shantsev, and R.G. Mints, *Phys. Rev. B* **74**, 220511(R) (2006).
5. F.L. Barkov, D.V. Shantsev, T.H. Johansen, P.E. Goa, W.N. Kang, H.J. Kim, E.M. Choi, and S.I. Lee, *Phys. Rev. B* **67**, 064513 (2003).
6. S. Treiber, C. Stahl, G. Schütz, and J. Albrecht. *Phys. Rev. B* **84**, 094533 (2011).
7. G.K. Perkins, J. Moore, Y. Bugoslavsky, L.F. Cohen, J. Jun, S.M. Kazakov, J. Karpinski, and A.D. Caplin, *Supercond. Sci. Technol.* **15**, 1156 (2002).
8. Valeria Braccini, *Ph.D. Thesis in Physics*, Università degli Studi di Genova (2003).
9. V.K. Vlasko-Vlasov, U. Welp, G.W. Crabtree, D. Gunter, V. Kabanov, and V.I. Nikitenko, *Phys. Rev. B* **56**, 5622 (1997).
10. E.H. Brandt, *Phys. Rev. B* **58**, 6506 (1998).
11. T. Schuster, H. Kuhn, E.H. Brandt, M. Indenbom, M.R. Koblischka, and M. Konczykowski, *Phys. Rev. B* **50**, 16684 (1994).
12. J. Karpinski, M. Angst, J. Jun, S.M. Kazakov, R. Puzniak, A. Wisniewski, J. Roos, H. Keller, A. Perucchi, L. Degiorgi, M.R. Eskildsen, P. Bordet, L. Vinnikov, and A. Mironov, *Supercond. Sci. Technol.* **16**, 221 (2003).